PREDICTION OF AERODYNAMICS CHARACTERISTICS AND AIRLOADS OF A GENERIC GEOMETRY WING

T. F. G. Costa, E. M. Belo
School of Engineering of Sao Carlos – University of Sao Paulo, Brazil

Keywords: *lifting line; finite wings; potential aerodynamics.*

Abstract

The purpose of this work is to present a mathematical model for the determination of three dimensional wings characteristics and airloads by using potential aerodynamics and experimental data of airfoils. The difficulty of determining aerodynamic characteristics of a wing increases if the shape changes from the conventional rectangular. The main idea of this study is to develop a computational method to calculate the lift, drag and moment coefficients against angle of attack, and the airload of a generic geometry wing. The final wing data must take into account the nonlinear phenomena such as stall.

The potential aerodynamics is based on the Prandtl lifting line theory, in which the wing is divided in several strips, and the lift comes from a line of vortices at ¼ of chord. Each strip uses the 2D airfoil characteristics. The use of a non-stationary wake to permit its roll-up completes the method.

1 Introduction

Some airplane characteristics as maximum lift coefficient ($C_{L\max}$) are left to the final stages of its design. A good prediction of these characteristics at the beginning, or parallel to other design tasks would influence the final configuration in a different way, and probably would result in a better airplane [1].

In this article it will be considered that a complete analysis of 3D (three-dimensional) properties of an airplane wing is to determine the distribution of the lift, drag and moment coefficients along semi-span (airloads, C_l, C_d and C_m *versus* $b/2$, respectively) and the total aerodynamic properties, as lift, drag and moment of the wing per angle of attack (C_L, C_D and C_M *versus* a). In all notations read downercase sub-script as local (2D) value, and uppercase sub-script as total wing (3D) value.

To three-dimensionalize the data from airfoil to the wing, the Prandtl's lifting line theory was used. The classical theory uses an infinite Fourier series representation of the airload distribution [2, 13 and 14]. The infinite series is usually truncated with a convenient number of terms. *van Dam et al* [1] use about 100 to 1000 terms, but uses planar wake. As the number of terms in the series must be equal to the number of horseshoe vortex used to represent the wing, a large number of elements increase excessively the computing time for solve wake position. So, the wing was divided into 10 to 50 elements and the load was simplified by a discrete presentation. The Fourier series was not used.

The 2D airfoil data, used in each element of the wing is obtained by wind tunnel test or viscous computational simulations [1].

The non-stationary wake was used to permit its roll-up, increasing precision on induced drag calculation [11 and 12].

2 Numerical Three-Dimensional Model

2.1 Lifting Line Method

The discrete lifting line method consists in subdivide the wing in N horseshoe vortex elements [2, 3, 4 and 5]. Each element has constant strength all along its extension,

including the wake, as in Figure 1. For simplicity, horseshoe vortex element will be called only element.
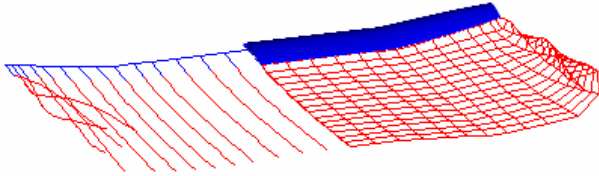
Figure 1 - Lifting line method

If a line segment represent a part of two or more elements (as in the case of two adjacent elements), the total circulation is the sum of the circulation of all elements in common.

The aerodynamic force (L_j) is a result of the flow crossing the line vortex at ¼ chord. The force on one element is given by equation (1) [2 and 3].

$$\vec{L}_j = r \Gamma_j \left(\vec{V}_j \times \vec{b}_j \right) \qquad j = 1, 2 \dots N \qquad (1)$$

where r = air density

Γ_j = element circulation

$\vec{V}_j$ = total velocity on center point of the spanwise segment of the element

$\vec{b}_j$ = element span (difference between final and initial points of the segment)

N = total number of elements

The component of L_j perpendicular to the free flow is the lift, and the component parallel to the free flow is the induced drag.
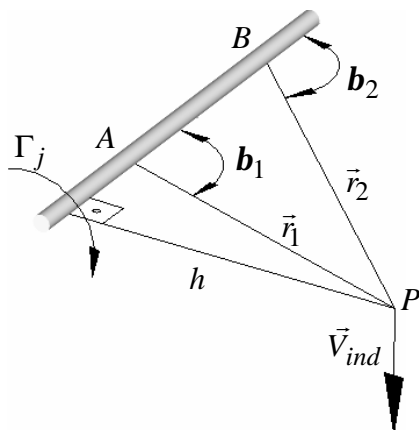
Figure 2 – Biot-Savart law

The induced velocity of one element on another is the sum of the velocity induced by each segment of the element. Biot-Savart's law describes the velocity induced by a vortex segment on a point, if the flow is potential [4].

As in Figure 2, the velocity induced ($\vec{V}_{ind}$) by AB segment on P is:

$$\vec{V}_{ind} = \frac{\Gamma_j}{4 p h} \left(\cos b_1 - \cos b_2 \right) \hat{e} \qquad (2)$$

where $\hat{e}$ is the unitary vector perpendicular to h and perpendicular to the segment.

With some mathematical treatment equation (2) becomes:

$$\vec{V}_{ind} = \frac{\Gamma_j}{4p} \frac{\vec{r}_1 \times \vec{r}_2}{|\vec{r}_1 \times \vec{r}_2|^2} \left(\frac{\vec{r}_1}{|\vec{r}_1|} - \frac{\vec{r}_2}{|\vec{r}_2|} \right) \cdot (\vec{r}_1 - \vec{r}_2) \qquad (3)$$

2.2 Coupling of Two-Dimensional Data to Three-Dimensional Geometry

To solve the load on wing, the data from airfoil must be known, and were connected do the three-dimendional model by the angle of attack in the element.

Figure 3 shows the base of this method.
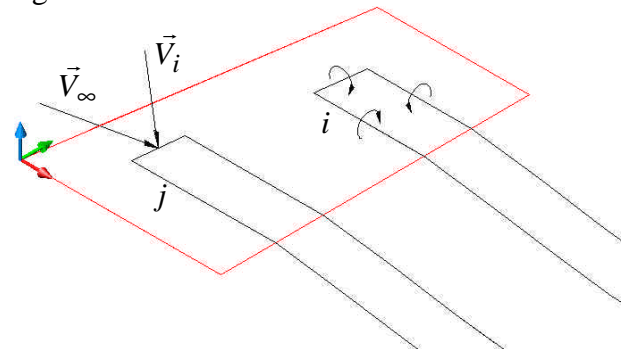
Figure 3 - Interations between horseshoe vortex

$$\vec{V}_{e_j} = \left(\vec{V}_\infty + \sum_i^N \vec{V}_i \right) \cdot \left(1\hat{i} + 0\hat{j} + 1\hat{k} \right) \qquad (4)$$

where $\vec{V}_{e_j}$ = total velocity induced by all elements of the model.

$\vec{V}_\infty$ = free flow velocity (same as model speed).

$\vec{V}_i$ = velocity induced by element i, as in Figure 3. It is calculated by equation (5)

$\hat{i}$ = unitary vector in airplane longitudinal direction, pointing to tail

$\hat{j}$ = unitary vector pointing to airplane right wing

$\hat{k}$ = unitary vector in vertical direction, pointing up.

$$\vec{V}_i = \sum_M \vec{V}_{ind} \qquad (5)$$

where $\vec{V}_{ind}$ = is obtained from equation 3

M = total of straight segments on element i

The reference for calculating the element angle of attack is the element chord direction. This direction ($\hat{c}$) is determined by:

$$\hat{c} = \frac{\hat{j} \times \hat{n}}{\left| \hat{j} \times \hat{n} \right|} \qquad (6)$$

where $\hat{n}$ = unitary vector normal to the element.

Finally, the element angle of attack ($\boldsymbol{a}_{e_j}$) is given by:

$$\boldsymbol{a}_{e_j} = \cos^{-1}\left(\frac{\hat{c} \cdot \vec{V}_{e_j}}{\left| \vec{V}_{e_j} \right|} \right) \qquad (7)$$

Considering the element lift coefficient as a function of angle of attack, the element strength may be calculated a:

$$\Gamma_j = \frac{\left| \vec{V}_{e_j} \right| S_j C_{l_j}}{2 \left| \vec{b}_j \right|} \qquad (8)$$

where S_j = element area

C_{l_j} = element lift coefficient

To connect the data from two-dimensional wing airfoil to the three-dimensional wing geometry, the function of the lift coefficient (equation (9)) is given by discrete data from other sources, as wind tunnel or a viscous simulation.

$$C_{l_j} = C_l(\boldsymbol{a}_{e_j}) \qquad (9)$$

To determine drag and moment coefficient, a similar relation is used:

$$C_{d_j} = C_d(\boldsymbol{a}_{e_j}) \qquad (10)$$

$$C_{m_j} = C_m(\boldsymbol{a}_{e_j}) \qquad (11)$$

Now the three-dimensional data from the whole wing can be found.

2.3 Non-Stationary Wake
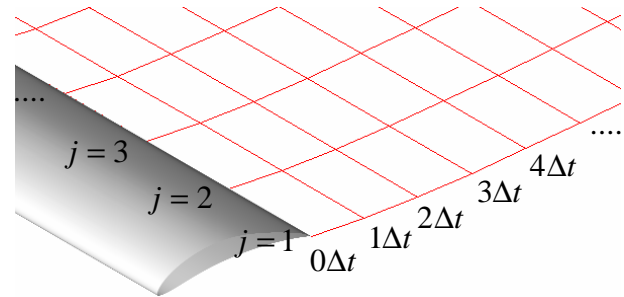
Figure 4 – Wake modeling

Each point of the wake is positioned behind other one by a Δt difference on time, as in Figure 4. The total points (j) in $\hat{j}$ direction is $N+1$.

As the strength of the horseshoe vortex is constant in all its extension (including the wake) the segments on Figure 4 in $\hat{j}$ direction have no circulation.

The positions of all points are described as a function of the forward point and the velocity on it:

$$(\vec{P}_j)_{t+\Delta t} = (\vec{P}_j)_t + \Delta t \cdot \vec{V}_{w_j} \qquad (12)$$

where $\vec{P}$ = vector indicating a wake point position. The subscript j = 1, 2, 3, … $N+1$ is the point ID along $\hat{j}$ direction

t = represents one line of the wake parallel to the span direction

$t + \Delta t$ = represents the line parallel to the span immediately afterward the t line

$\vec{V}_{w_j}$ = is the total velocity on the point in t line. It is calculated as follows:

$$(\vec{V}_{w_j})_t = \vec{V}_\infty + \sum_{i=1}^{N} \vec{V}_i \qquad (13)$$

where $\vec{V}_i$ is the total velocity induced on point (t, j), calculated by equation (5).

The final position of the entire wake is obtained iteratively.

2.3 Iterative Procedure

2.3.1 Load Iterations
If the initial load is given, and the wake position is known, each iteration step is determined by:

$$step = C_{damp}[(C_{l_j})_{k+1} - (C_{l_j})_k] \qquad (14)$$

where C_{l_j} = lift coefficient of element j

k = indicates the iteration

C_{damp} = artificial damping coefficient

An artificial damping was added to the equation because the method showed to be unstable. A value of 0.01 for C_{damp} was enough to guarantee the convergence.

The next lift distribution (load) is given by:

$$(C_{l_j})_{k+1} = (C_{l_j})_k + step \qquad (15)$$

Iterations stops when the error becomes smaller than an established value. The error is assumed as:

$$error = \sqrt{\sum_{j=1}^{N}\{[(C_{l_j})_{k+1} - (C_{l_j})_k]^2\}} \qquad (16)$$

2.3.2 Wake Iterations
If the load is known, and the initial wake position is given, equation 12 is repeated for all wake points until the error on wake geometry met a determined value.

The error on wake geometry is calculated similarly to equation (16), but it is used the

difference between the same point position in two different iterations.

2.3.3 Model Convergence
As the wing load depends on the wake position, and the wake position depends on the wing load, the final solution of this system is obtained when both respect each other.

To find this solution, the load and wake iterations were repeated until both iterations respect error parameters with only one step. This procedure can be seen on the following diagram:
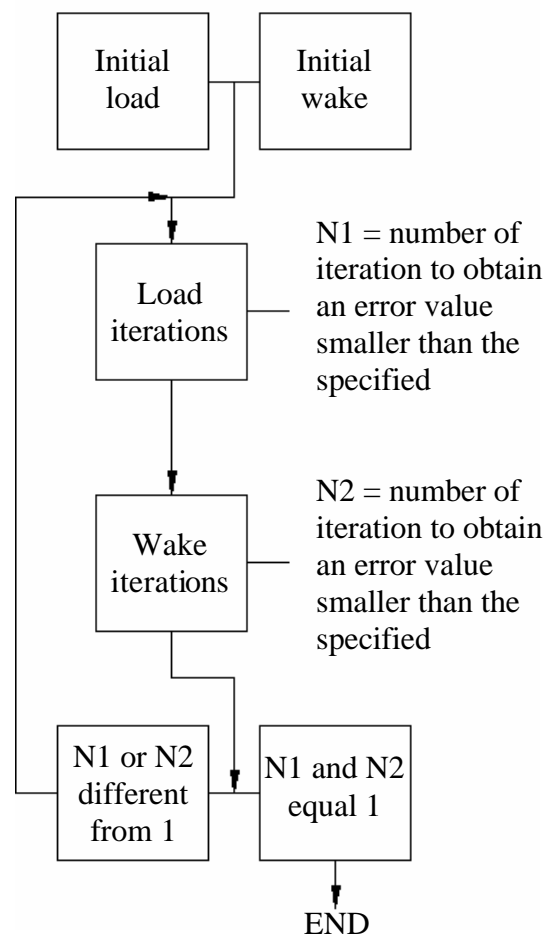
Figure 5 – Final solution procedure

2.4 Initial load and wake

To start the entire iterative program, an initial load and wake are necessary.

A plane wake was used and shows to be a good starting point. It converged in all cases.

As initial lift load, it was first adopted a C_l distribution corresponding to the local angle of

attack distribution considering only the free flow velocity on each element. This initial load converged only for some specific cases. The solution diverged because this initial load has much circulation concentrated on wing tip. To correct this problem, a smaller load needs to be used. A load with half of the C_l used before in each position was adopted and work.

2.5 Solution Precision

It is intuitive that as more elements used to describe a wing geometry, more precise will be the solution.

To quantify the precision, the wing lift coefficient (C_L) at stall angle was used, as in Figure 6

Taking the wing on Figure 6 as example, the difference in C_L for change the number of elements of 50 to 42 is about 0.07%. For changing to 15 elements, C_L changes 0.88%.

Considering acceptable an error smaller than 1.00% in maximum C_L, the recommended element aspect ratio is about 0.33, or smaller

(i.e., the element span is smaller than one third of the chord of the wing on that position).
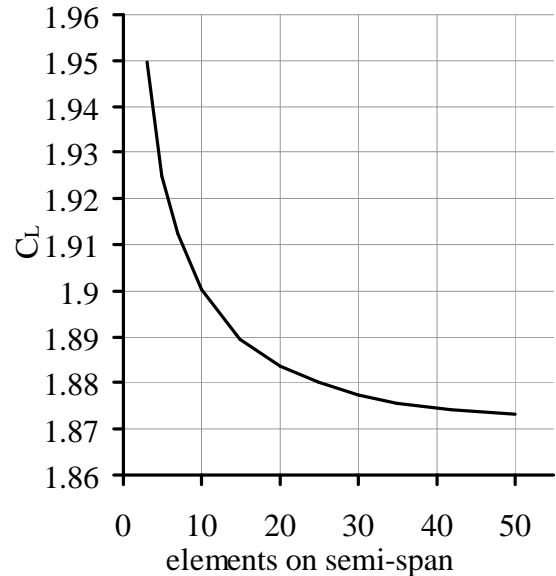
Figure 6 - Variation of C_{Lmax} with respect to number of elements of a rectangular wing with aspect ratio 10 and airfoil Eppler E423
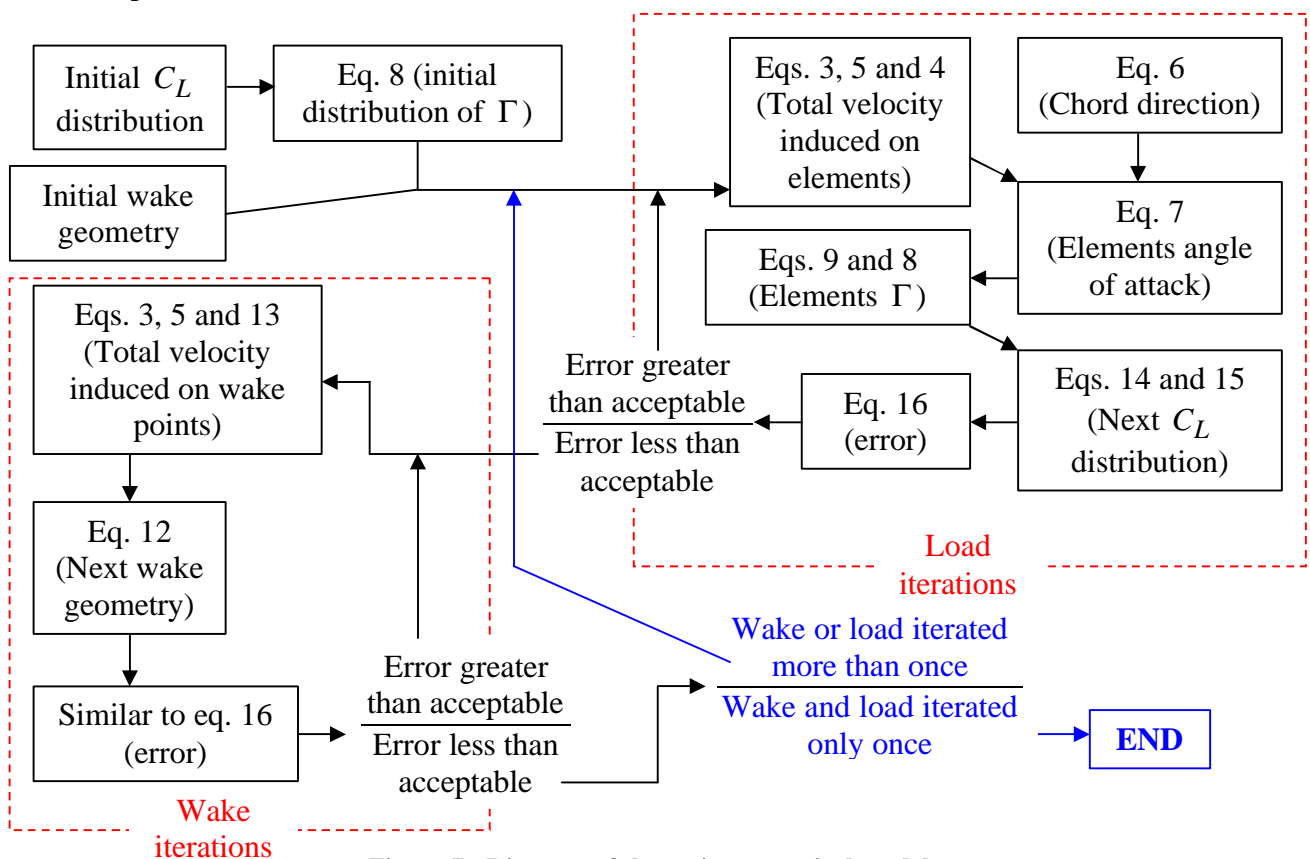
Figure 7 - Diagram of the entire numerical model

2.6 Drag and Moment

As the solution presents the distribution of two-dimensional properties along semi-span, it is possible to determine drag and moment loads.

After solve the flow over a model, the distribution of angle of attack is known. Using equations (10) and (11) for drag and moment coefficients (C_d e C_m) of the airfoil, the total wing coefficients can be found (C_D e C_M)

3 Simulations and Results

With the objective of verifying the results of this method, several simulations were done. These simulations intended to check aerodynamics properties against wing geometry.

3.1 Aspect Ratio Influence on C_L x a curve

Several wings were simulated with Selig S1223 airfoil, because this is a high lift airfoil with nonlinear C_l x a curve at low angle of attack.

So it is possible to verify three-dimensional behavior on stall and other non linearity. Figures 8 and 9 show the results of simulations. Note that with the decrease of aspect ratio, the stall angle increases and the maximum C_L decreases. This behavior is already known and was proved experimentally [6 and 7].
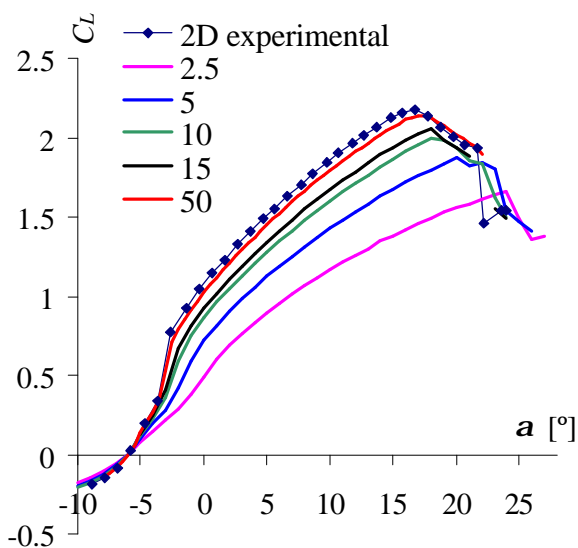
Figure 8 - C_L x a curves for several aspect ratios.

The two-dimensional data from Selig S1223 airfoil at Reynolds 171400 was taken from University of Illinois at Urbana-Champaign web site [8].
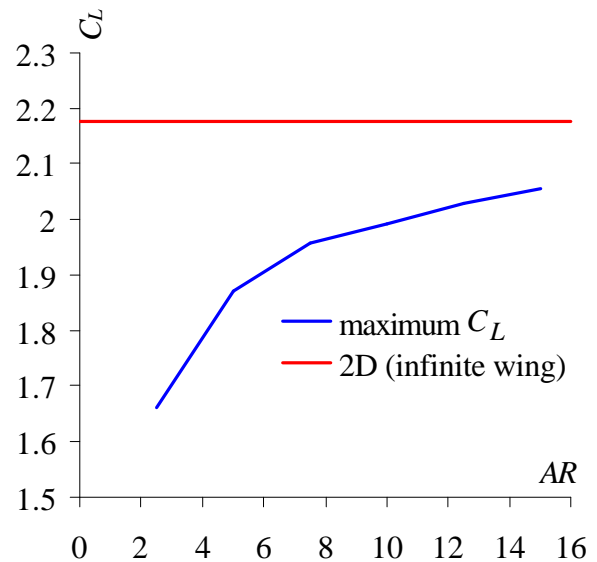
Figure 9 – Variation of maximum C_L per aspect ratio for rectangular wing with Selig S1223 airfoil [8]

3.2 Sweep Angle Influence on Load
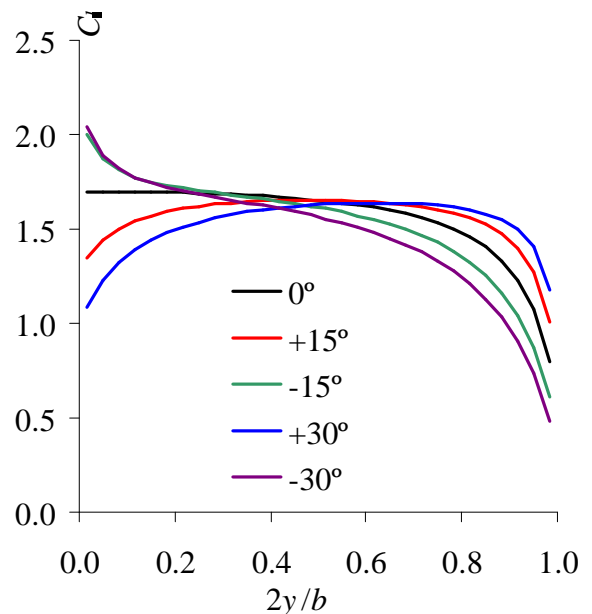
Figure 10 - C_l distribution for several sweep angles of a wing with aspect ratio 10 airfoil Eppler E423 [9], at 10º of angle of attack

Five constant chord wings with same span were simulated. The sweep angle was modified as in

Figure 10 (all elements were keep with aspect ratio 0.33), and shows the expected behavior [6].

It is possible to note the great C_l on wing tip for wings with positive sweep. It explains the problem of tip stall common in this type of wings. The tip stall increases the chances of spin, so it's better to avoid it [7].

The two-dimensional data from Eppler E423 airfoil at Reynolds 199400 was taken from University of Illinois at Urbana-Champaign web site [9].

3.3 Plan Form Geometry Influence on Load

Several simulations were done to study the taper ratio influence on load. The same parameters of sweep analysis were used (wing aspect ratio 10, elements aspect ratio 0.33, airfoil Eppler E423, and wing angle of attack 10 °).

Results are shown in Figure 11.
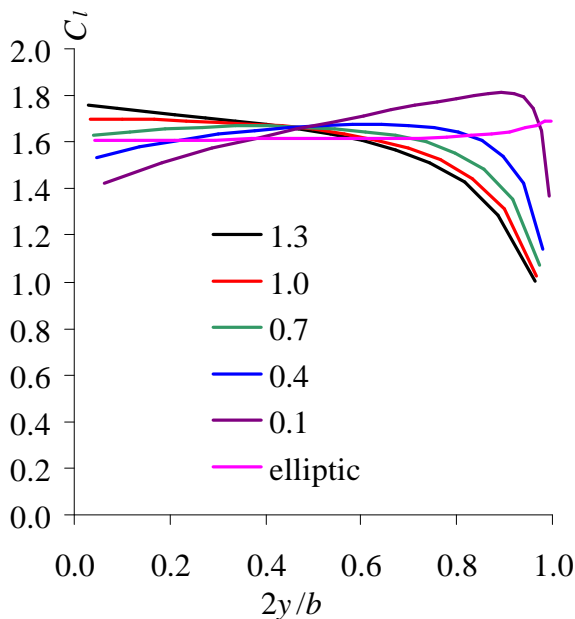
Figure 11 - C_l distribution for several taper ratios of a wing with aspect ratio 10 airfoil Eppler E423 [9], at 10º of angle of attack

The results had shown that taper ratio smaller than one has same behavior of positive sweep angle [6 and 7].

The elliptic plan form was simulated and had shown a load of C_l distribution almost rectangular, as expected. This load respects the

elliptic circulation distribution that elliptic wing must have [7].

3.4 Entire Aircraft Analysis

An entire airplane was simulated to compare with the real model.

The airplane chosen was a prototype of Team of School of Engineering of Sao Carlos for *SAE Brasil AeroDesign Competition* [10]. Information about the competition rules can be found on *SAE Brasil* internet web site [10]. The objective of this competition is designing a cargo airplane to take-off with the largest payload as possible.

The method present in this article was used to preview airplane aerodynamic, loads and stability characteristics.

The airplane is basically as in Figures 12 and 13.

Wing:
Span = 157.5 inches
Chord = 14.8 inches
Airfoil: Eppler E423
Elevator:
Span = 39.4 inches
Chord = 7.9 inches
Airfoil: Clark-Y
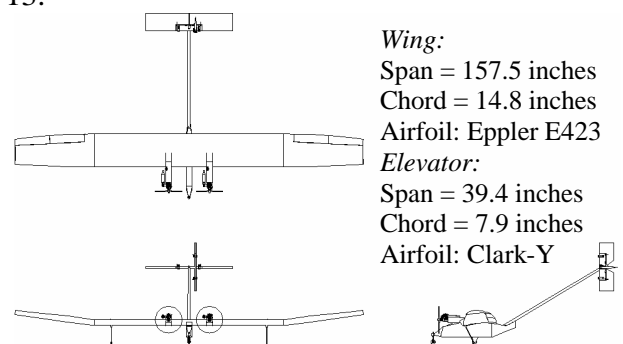
Figure 12 – Three views from airplane chosen

Figure 13 – Isometric render view from airplane

The whole aircraft was modeled and the results were used during airplane design.

The payload lifted by the aircraft was close to the preview. The error was due to mistakes in rolling friction determination experiment.

The value of lift and drag was assumed to be correct, as the airplane behavior was the same as predicted.
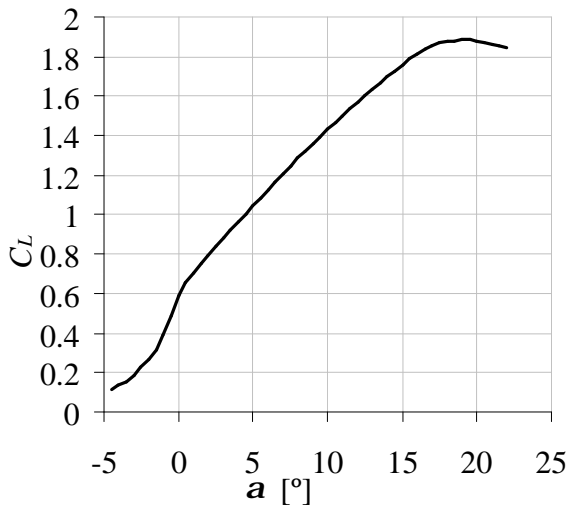
Figure 14 - C_L **x** **a** **for trimmed airplane**
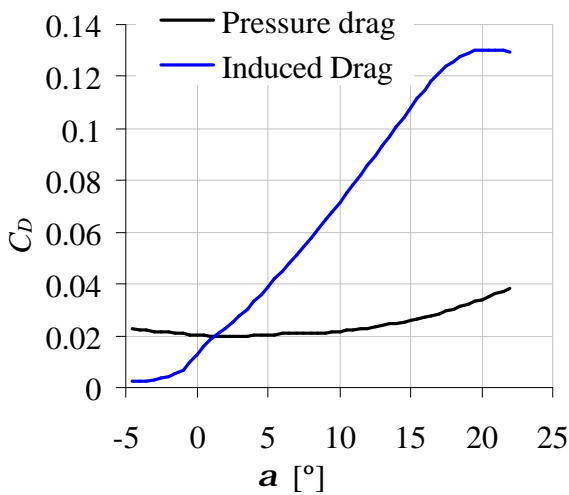
Figure 15 - C_D **x** **a** **for trimmed airplane**
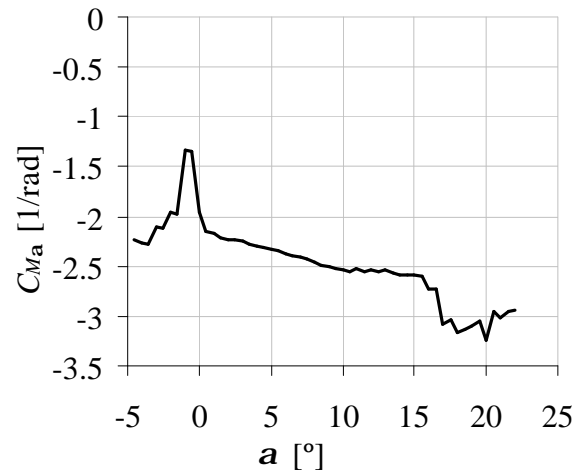
Figure 16 – C_{Ma} **x** **a** **for trimmed airplane,**
C_{Ma} **= Derivative of** C_M **with respect to** **a**
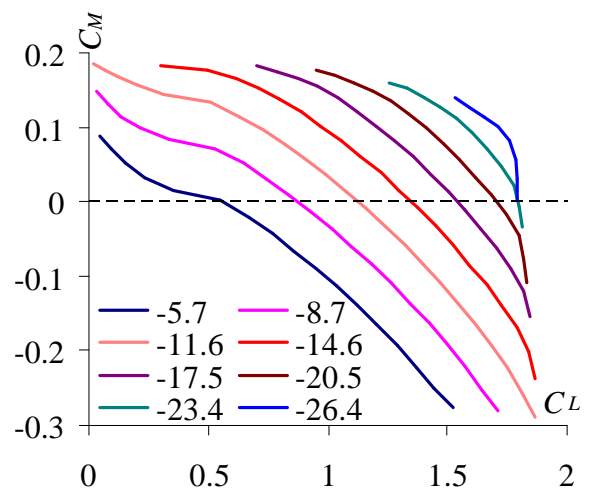
Figure 17 – Trim cross plot (each line represents a deflection on elevator angle in degrees)
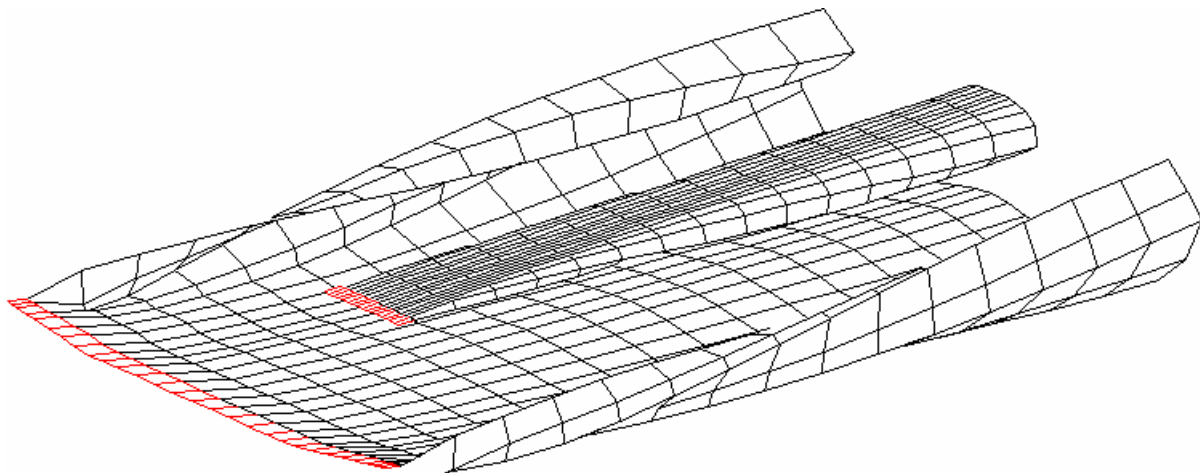
Figure 18 - Airplane trimmed at take-off condition (14º of angle of attack)

All curves (except Figure 17) were obtained for trimmed conditions, i.e. concerning the horizontal stabilizer down force.

All non-linearities of wing and elevator airfoils appeared in results.

The trim cross plot (Figure 17) was used to compare the numerical model to the real prototype. The trim angle on elevator were measured on ground, after trimming flights, and it was noted an error about 1º. This error was considered acceptable, concerning the simplicity of the numerical equation, and the complexity of the real model.

4 Conclusions

The numerical method presented in this article is adequate for solving in pc computers without the need for computer clusters, as usually needed for viscous CFD (Computer Fluid Dynamics) solving. So, it is a light and fast solution for previewing the three-dimensional characteristics and airloads of an aerodynamic model, including non-linearities as stall.

The stall characteristics are usually problematic when using lifting-line theory. This occurs due to C_l x $\textbf{\textit{a}}$ curve be not invertible when considering stall (for a given C_l value there are two possibilities of $\textbf{\textit{a}}$ values). This may cause not unique solution. Because of this, the equation 9 must be used entering $\textbf{\textit{a}}$. For each $\textbf{\textit{a}}$ there is only one value of C_l as result. Due to numerical fluctuations, the first element to stall on wing may vary. In other words, the load solution may not be unique. This variation of the first element to stall occurs always around the region with greatest C_l on the wing. So, this numerical problem had not much influence on total C_L of the wing, which solution can be considered unique. As example, take the solution for aspect ratio 50 shown on Figure 8. A wing with this aspect ratio has a load distribution almost rectangular. Due to these numerical fluctuations, is difficult to preview which is the first element to stall. However, this first element is always near the wing root. On the other hand, the aspect ratio is so large that

the C_L x $\textbf{\textit{a}}$ curve is almost the 2D curve (or infinite wing solution), concluding that the total C_L solution is probably correct.

Unfortunately, experiments with measurement of static pressure over the wing to verify the precision on load calculation were not done for these wings simulated. Although it is expected that it is correct, due to results presented in Figures 10 and 11.

The main goal of the method presented here was to determine aerodynamics non linear properties of a 3D model using potential methods. A lot of simulations were done to compare data and verify where the non-linearities appear. A complete aircraft was analyzed and the airfoil non linear properties appear on all result curves. This method shows to be simpler than the classical one with Fourier series, and accepts well non linear parameters.

References

[1] van Dam C P, Vander Kam J C and Paris J K. Design-oriented high-lift methodology for aviation and civil transport aircraft. *Journal of aircraft*, Vol. 38, No. 6, pp 1076-1084, 2001.

[2] Anderson J D. *Fundamentals of aerodynamics*. 2nd edition, McGraw-Hill International Editions, 1991.

[3] Houghton E L and Carpenter P W. *Aerodynamics for engineering students*. 1st edition, Elsevier Butterworth-Heinemann, 2003.

[4] Katz J, Plotkin A. *Low-Speed aerodynamics*. 2nd edition, Cambridge University Press, 2001.

[5] Morino L. *Computational methods in potential aerodynamics*. 1st edition, Computational Mechanics Publications, 1985.

[6] Hoerner S F. *Aerodynamic and hydrodynamic lift*. 1st edition, Mrs. Liselotte A. Hoerner, 1975

[7] Raymer D P. *Aircraft design: a conceptual approach*. 2nd edition, AIAA, 1992.

[8] Selig M. *UIUC Low-Speed Airfoil Tests*. http://www.ae.uiuc.edu/m-selig/pub/LSATs/AppendedFiles_vol1/LIFT01.TXT (30 march, 2006)

[9] Selig M. *UIUC Low-Speed Airfoil Tests*. http://www.ae.uiuc.edu/m-selig/pub/LSATs/AppendedFiles_vol2/LIFT02.TXT (30 march, 2006)

[10] SAE Brasil, http://www.saebrasil.org.br/ (01/06/2005)

[11] Smith S C. Induced drag computations on wings with accurately modeled wakes. *Journal of aircraft*, Vol. 34, No. 2, pp 253-255, 1997.

[12] Smith S C. Computation of induced drag for elliptic and crescent-shaped wings. *Journal of aircraft*, Vol. 30, No. 4, pp 446-452, 1993.

[13] Phillips W F. Lifting-line analysis for twisted wings and washout-optimized wings. *Journal of aircraft*, Vol. 41, No. 1, pp 128-135, 2004.

[14] Phillips W F, Alley N R, Goodrich W D. Lifting-line analysis of roll control and variable twist. *Journal of aircraft*, Vol. 41, No. 5, pp 1169-1176, 2004.